New Journal of Physics
The open access journal for physics

Ab initio spin-resolved photoemission and electron pair emission from a Dirac-type surface state in W(110)

H Mirhosseini[1,2,5], F Giebels[3], H Gollisch[3], J Henk[4] and R Feder[1,3]

[1] Max Planck Institute of Microstructure Physics, Weinberg 2, D-06120 Halle (Saale), Germany
[2] Institute of Inorganic and Analytical Chemistry, Johannes Gutenberg University, D-55122 Mainz, Germany
[3] Theoretical Solid State Physics, University Duisburg-Essen, Campus Duisburg, D-47048 Duisburg, Germany
[4] Institute of Physics—Theoretical Physics, Martin Luther University Halle-Wittenberg, D-06099 Halle (Saale), Germany
E-mail: mirhosse@uni-mainz.de

New Journal of Physics **15** (2013) 095017 (15pp)
Received 8 May 2013
Published 26 September 2013
Online at http://www.njp.org/
doi:10.1088/1367-2630/15/9/095017

Abstract. The spin texture of a Dirac-type surface state in W(110) lends itself to study spin-dependent effects in electron spectroscopies that show up very clearly. Firstly, we report on spin-resolved photoemission calculations and separate the spin polarization that is attributed to the initial state from that induced by the photoemission process itself. This disentanglement allows one to map spin textures of spin-polarized initial states using circular dichroism, for example from Dirac surface states in topological insulators. Secondly, we demonstrate the mapping of spin-polarized states by spin-dependent two-electron emission. Selecting highly polarized initial states, this spectroscopy can furthermore probe the spin dependence of the exchange-correlation hole.

[5] Author to whom any correspondence should be addressed.

Contents

1. Introduction

Topological insulators are a fascinating new class of materials [1]. In particular, strong topological insulators show a surface state with unique properties at the center of the surface Brillouin zone [2]: it bridges the fundamental band gap, disperses linearly and exhibits a Rashba-type spin texture [3–5]. These features have led to an extensive ongoing search for new topologically non-trivial materials (e.g. [6–9]). But also well-known materials are being re-investigated with respect to surface states that show some features of a 'true' Dirac surface state. Recently, a Dirac-type surface state (DSS) has been identified at the (110) surface of tungsten [10–12]. Although known for some time [13], its Dirac properties have been proven experimentally by spin- and angle-resolved photoelectron spectroscopy [14] by Miyamoto and co-workers [10]. These findings have been complemented theoretically by first-principles calculations [15, 16].

It is these salient properties of the DSS in W(110) that lend support for investigations of spin-driven effects in electron spectroscopies [17–19]. In this paper we elaborate on how these show up in spin- and angle-resolved photoemission (SARPES) [20, 21] and in electron pair emission $(e, 2e)$ [22, 23].

The first spectroscopy covered in this paper is SARPES. The spin of the DSS (i.e. the initial state in SARPES) is completely in-plane. The photoemission process itself lowers the symmetry of the entire setup and, hence, allows for a non-zero perpendicular component of the photoelectron's spin polarization. While this effect has been addressed briefly for linearly polarized light in [16], we focus in this paper on circularly polarized light. Questions to be answered comprise the effect of 'optical orientation' [24] on the photoelectron spin in dependence on the symmetry of the setup. Furthermore, mapping the spin texture of the Dirac state in three-dimensional topological insulators [1, 25–27] by circular dichroism experiments [28, 29] is challenging, due to the specific occupied surface electronic structure of the prototypical systems (i.e. the bichalcogenides Sb_2Te_3, Bi_2Te_3, Bi_2Se_3). In particular, the Dirac surface state is very close (in $(E, \boldsymbol{k})$) to bulk states and the energy range accessible by photoemission is rather small (the fundamental gap is less than 0.2 eV wide). This is different for the DSS in W(110) that 'resides' in a wide band gap and shows features strongly reminiscent

of those of a true Dirac state. Hence being—roughly speaking—'isolated', this surface state represents a prototypical system for studying the joint effect of 'optical orientation' and spin texture on circular dichroism of Dirac-type states [29, 30]. We provide a method to disentangle the origin of the photoelectron's spin polarization—initial state or optical orientation—by taking appropriate intensity differences which may prove useful also for studying Dirac states of topological insulators.

Complementary to photoemission, we explore the spin-polarized surface states by means of a second spectroscopic method: electron-induced emission of correlated electron pairs, commonly referred to as $(e, 2e)$ spectroscopy (see [15] and references therein). The spin orientation of the incident low-energy electrons relative to the surface state electrons, with which they collide, entails either parallel or anti-parallel spins of the two outgoing electrons. The two electrons are therefore correlated either by exchange and Coulomb interaction or by Coulomb interaction only, which implies a fundamental difference between the $(e, 2e)$ reaction cross sections (intensities) in the two cases. This spin dependence allows a spin-resolved mapping of the surface state dispersion relations. We demonstrate this by relating spin-dependent $(e, 2e)$ spectra to the underlying spectral density in the surface layer resolved with respect to spin and spatial parity. Selecting on such a map a highly spin-polarized initial state and keeping it fixed, momentum distributions of the emitted electrons exhibit a large exchange-correlation hole for parallel spins and a much smaller correlation hole for anti-parallel spins.

The paper is organized as follows. Theoretical aspects are addressed in section 2. Results are discussed in section 3, focusing on SARPES in section 3.2 and on $(e, 2e)$ in section 3.3. We conclude with section 4.

2. Theoretical aspects

2.1. Electronic structure calculations

The electronic structure calculations were performed within the framework of the local spin-density approximation to density-functional theory. Our computations rely on the layer Korringa–Kohn–Rostoker (KKR) method for spin-dependent systems [31, 32]. In this relativistic approach, spin–orbit coupling is accounted for by solving the Dirac equation. The site-dependent potentials have been obtained by full-potential augmented plane waves (FLAPW) calculations[6] and subsequently transferred to our KKR code. Since all the results presented in this paper rely on the computational setup used earlier, it is sufficient to sketch its main ingredients here; for details see [15].

The W(110) surface is treated as a semi-infinite system, in which the potential in the outermost three layers differs from that of the bulk-like layers (with bulk potential). The top layer is relaxed inward by $\Delta d = -3\%$ with respect to the bulk interlayer distance, in agreement with low-energy electron diffraction (LEED) and surface x-ray diffraction analyses [33, 34]. The image-potential barrier is taken as a smooth interpolating function [35].

From the layer-resolved Green function G_{ll} of the entire system, we calculate the spectral density $N_l(E, \boldsymbol{k})$ for layer l at energy E and surface-parallel wavevector $\boldsymbol{k}$

$$N_l(E, \boldsymbol{k}) = -\frac{1}{\pi} \lim_{\eta \to 0^+} \Im \mathrm{Tr}\, G_{ll}(E + \mathrm{i}\eta, \boldsymbol{k}). \tag{1}$$

[6] The Jülich FLAPW code family: FLEUR. Forschungszentrum Jülich, D-52425 Jülich, Germany.

Table 1. Effect of mirror operation m_{xz} on the photoelectron spin vector $\boldsymbol{s}. = (s_x, s_y, s_z)$, the vector potential $\boldsymbol{A} = (A_x, A_y, A_z)$ of the incident light in photoemission, and its helicity σ in the case of circular polarization. The wavevector $\boldsymbol{k}$ is along the k_x-axis ($k_y \equiv 0$).

Identity	1	s_x	s_y	s_z	A_x	A_y	A_z	$\sigma_\pm$
Reflection at xz plane	m_{xz}	$-s_x$	s_y	$-s_z$	A_x	$-A_y$	A_z	$\sigma_\pm$

By taking appropriate partial traces, the spectral density can further be decomposed with respect to angular momentum and spin projection. When discussing the spin texture of the Dirac surface state, we rely on spin differences

$$S_{l\mu}(E, \boldsymbol{k}) \equiv S_l(E, \boldsymbol{k}; \uparrow_\mu) - S_l(E, \boldsymbol{k}; \downarrow_\mu) \tag{2}$$

of spin-dependent spectral densities that are resolved with respect to the chosen spin quantization axis μ.

2.2. *Photoemission calculations*

SARPES spectra were calculated within the relativistic one-step model of photoemission [31, 36, 37], using our layer KKR computer code. Spin–orbit coupling, boundary conditions and the transition matrix elements between the initial state and the time-reversed spin-polarized LEED state (that describes the outgoing electron) are fully taken into account. The result of the computation is the spin density matrix $\underline{\underline{\boldsymbol{\rho}}}$ of the photoelectron that depends on the kinetic energy E and the detection direction of the photoelectron (expressed in terms of the wavevector $\boldsymbol{k}$). It gives the intensity $I = \mathrm{tr}\underline{\underline{\boldsymbol{\rho}}}$ and the spin polarization $s_\mu = \boldsymbol{\mu} \cdot \mathrm{tr}(\underline{\underline{\boldsymbol{\sigma}}}\,\underline{\underline{\boldsymbol{\rho}}})/I$ of the chosen spin quantization axis $\boldsymbol{\mu}$ ($\underline{\underline{\boldsymbol{\sigma}}}$ vector of Pauli matrices).

Excitation of the DSS by linearly polarized light has been investigated earlier [16]. In this paper, we focus on circularly polarized light (helicity $\sigma_\pm$) with a photon energy of 21.22 eV ($\mathrm{He_I}$); this particular energy was chosen because it is available both in synchrotron radiation facilities and from rare-gas discharge lamps in a laboratory. We investigate three setups—$\mathcal{A}$, $\mathcal{B}$ and $\mathcal{C}$—with decreasing degree of symmetry. While setup $\mathcal{A}$ is for normal incidence, $\mathcal{B}$ is for off-normal incidence within the $\overline{\mathrm{H}}$– $\overline{\Gamma}$– $\overline{\mathrm{H}}$ mirror plane of the surface ([001] direction). In both cases we focus on electron detection in the $\overline{\mathrm{H}}$– $\overline{\Gamma}$– $\overline{\mathrm{H}}$ mirror plane in which the surface state shows almost linear and strong dispersion. Setup $\mathcal{C}$ is for off-normal incidence and electron detection in [$\bar{1}$11] direction ($\overline{\mathrm{S}}$– $\overline{\Gamma}$– $\overline{\mathrm{S}}$) which is *not* a mirror plane. The surface state shows strong dispersion in this plane as well [10]. It becomes 'flattened' along $\overline{\mathrm{N}}$– $\overline{\Gamma}$– $\overline{\mathrm{N}}$ [11]. For $\mathcal{B}$ and $\mathcal{C}$ the polar angle of incidence ϑ_{ph} is chosen as 45°.

In setups $\mathcal{A}$ and $\mathcal{B}$, the spin polarization of the Dirac surface state is fully aligned perpendicular to the mirror plane. Considering as an example an xz mirror plane ($\boldsymbol{s}$ in table 1), s_y does not change sign upon reflection and, hence, is allowed non-zero, in contrast to s_x and s_z. The photoemission process lowers this symmetry restriction because the electric field $\boldsymbol{A}$ of the light has to be considered in addition ($\boldsymbol{A}$ in table 1). For circularly polarized light incident within the xz plane, the electric field vector can be expressed as

$$\boldsymbol{A} = (A_x, A_y, A_z) \propto (\cos\vartheta_{\mathrm{ph}}, \pm\mathrm{i}, \sin\vartheta_{\mathrm{ph}}). \tag{3}$$

In particular, A_y changes sign upon reflection m_{xz}: left-handed circular polarized light is turned into right-handed circular polarized light, and vice versa ($\sigma_\pm \to \sigma_\pm$ in table 1). As a consequence, the total photocurrent I is unchanged with respect to reversal of the light helicity: there is no circular dichroism [38]. Furthermore, all spin components of the photoelectron are allowed non-zero but s_x and s_z change sign upon helicity reversal while s_y does not. In a schematic notation, $(I; s_x, s_y, s_z; \sigma_\pm) = (I; -s_x, s_y, -s_z; \sigma_\pm)$ holds.

In setup $\mathcal{C}$, both light incidence and electron detection are *not* within a mirror plane of the surface, leading in general to circular dichroism; furthermore, all Cartesian components of the photoelectron's spin polarization $\boldsymbol{s}$ may be non-zero.

2.3. $(e, 2e)$ calculations

We employed a relativistic KKR-type formalism, which has been presented in detail in earlier work [22, 39]. The basic ingredients are four one-electron states $|i\rangle$ (with $i = 1, 2, 3, 4$), which are obtained as solutions of the Dirac equation with a complex potential and are characterized by energies E_i, surface-parallel momenta $\boldsymbol{k}_i$ and Rashba component spin labels $\sigma_i = \pm$. In the $(e, 2e)$ process, the Coulomb interaction induces a transition from an initial two-electron state $|1, 2\rangle$, which is an antisymmetrized product of the primary electron state $|1\rangle$ and the valence electron state $|2\rangle$, to a final two-electron state representing the two emitted electrons. $|3, 4\rangle$ is an approximate solution of a two-particle Dirac equation with the electron–electron interaction approximated by a screened Coulomb interaction. Being of course also antisymmetric with respect to interchanging the two electrons, it involves essentially products of the two one-electron states $|3\rangle$ and $|4\rangle$ and a Coulomb correlation factor. For details we refer to [39]. An important property of the $(e, 2e)$ process is the conservation of energy and parallel momentum:

$$E_1 + E_2 = E_3 + E_4, \quad \boldsymbol{k}_1 + \boldsymbol{k}_2 = \boldsymbol{k}_3 + \boldsymbol{k}_4 + \boldsymbol{g}, \tag{4}$$

where $\boldsymbol{g}$ is a surface reciprocal lattice vector.

The spin-resolved $(e, 2e)$ reaction cross sections 'intensities' can be expressed in a golden rule form with Coulomb matrix elements between the above initial and final two-electron states. Denoted by $I^{\sigma_1}_{\sigma_3\sigma_4}$, they involve a sum over the valence electron spin labels σ_2 and depend explicitly on the spin labels of the incoming and the two outgoing electrons. For parallel spins ($\sigma_3 = \sigma_4$), the $I^{\sigma_1}_{\sigma_3\sigma_4}$ contain both exchange and Coulomb interaction between the two emitted electrons, whereas for antiparallel spins, they contain only the Coulomb interaction. Further, they are in general functions of E_i and $\boldsymbol{k}_i$, with $i = 1, 3, 4$. For fixed E_i and $\boldsymbol{k}_i$, 4 implies definite valence electron energy and parallel momentum, i.e. one can map the dispersion relation of the valence electron states.

3. Results and discussion

3.1. Dirac-type surface state

As a prerequisite for discussing the electron spectroscopies, we recall briefly the salient properties of the DSS. We focus on the directions in which this state disperses strongly [11]. Along $\overline{\text{H}}$– $\overline{\Gamma}$– $\overline{\text{H}}$ (left in figure 1), the dispersion is almost linear, while it becomes slightly parabolic along $\overline{\text{S}}$– $\overline{\Gamma}$– $\overline{\text{S}}$ (right in figure 1). Its Dirac point shows up at E_F–1.25 eV and $\overline{\Gamma}$, in agreement with experiment [10, 12]. The orbital decomposition of the top layer's spectral

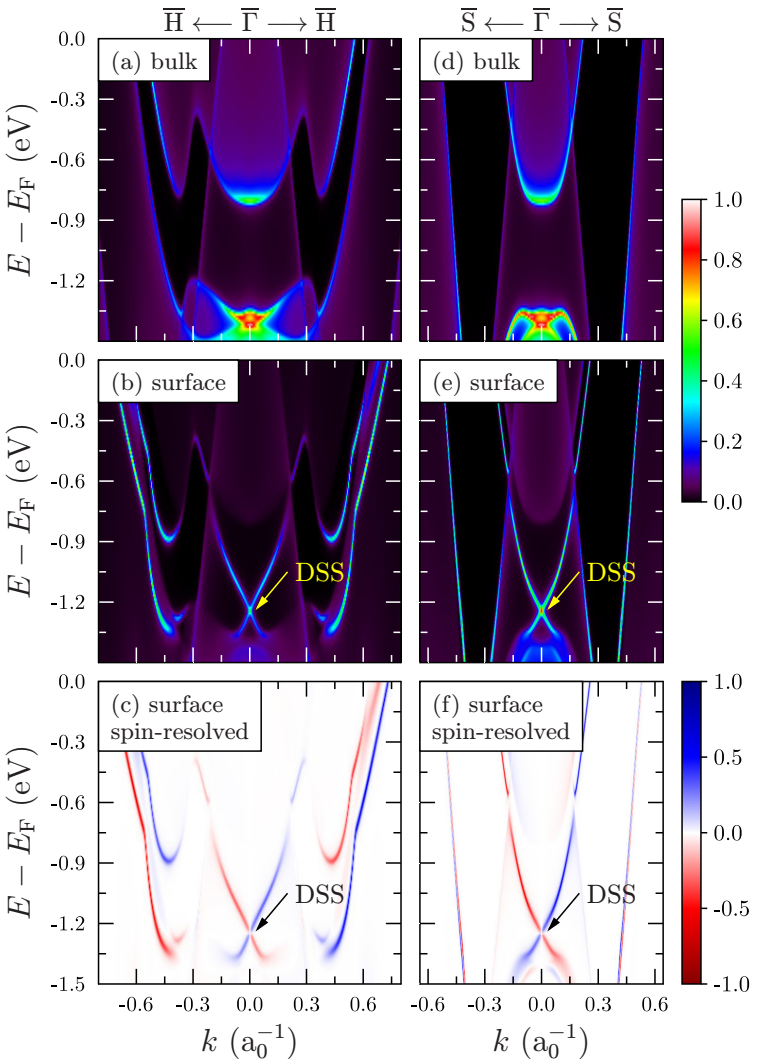

Figure 1. Electronic structure of W(110) for wavevector $\boldsymbol{k}$ along $\overline{\mathrm{H}}$– $\overline{\Gamma}$– $\overline{\mathrm{H}}$ ((a)–(c), left) and along $\overline{\mathrm{S}}$– $\overline{\Gamma}$– $\overline{\mathrm{S}}$ ((d)–(f), right). Normalized spin-integrated spectral densities are shown as color scale for a bulk layer ((a), (d)) and for the topmost surface layer ((b), (e)). The red–white–blue color scale for (c) and (f) displays data for negative-zero-positive normalized spin differences $S_{\mathrm{S}\mu}(E, \boldsymbol{k})$, with μ the Rashba component of the spin polarization. The spin polarization of the DSS is as large as 90% (in absolute value) close to the Dirac point. a_0 Bohr radii, E_F Fermi energy.

density yields that the surface state belongs to the Σ_1 (single-group) representation[7], with the by far largest contribution from d_{z^2} orbitals.

The spin texture is of Rashba-type, as dictated by point group and time-reversal symmetry, namely in-plane and perpendicular to $\boldsymbol{k}$ (this spin-polarization component is usually termed 'the Rashba component'). Time-reversal symmetry dictates a spin reversal upon turning $\boldsymbol{k}$ into $-\boldsymbol{k}$

[7] There is a single double-group representation, Σ^5, for the point group $2mm$ ($C_{2\mathrm{v}}$ in Schoenflies notation) [40, table B.10].

(cf the red–blue asymmetry in panels (c) and (f) of figure 1). The degree of spin polarization is about 90% (in absolute value) close to the Dirac point. It exceeds that of the Dirac surface state in the topological insulator Bi_2Te_3 (about 60% [27, 41]). Within this respect, the Dirac surface state of W(110) is closer to modeled Dirac states [42] than those in bichalcogenide topological insulators, thus lending itself for investigations of spin–orbit effects in electron spectroscopies from strongly spin-textured surface states [25, 43].

3.2. Spin-resolved photoemission

In the following, we discuss the evolution of photoelectron's spin texture and of circular dichroism when lowering the symmetry of the SARPES setup ($\mathcal{A} \rightarrow \mathcal{B} \rightarrow \mathcal{C}$). We also show how to disentangle the spin polarization from the initial state from that due to optical orientation.

Due to the symmetry relation $(I; s_x, s_y, s_z; \sigma_\pm) = (I; -s_x, s_y, -s_z; \sigma_\pm)$ that holds for setups $\mathcal{A}$ and $\mathcal{B}$, it is sufficient to present only results for one helicity (here: σ_+); the numerical results are fully in line with these transformations. For normal incidence (setup $\mathcal{A}$, left in figure 2), the intensity distribution is symmetric about $\overline{\Gamma}$, i.e. $I(\boldsymbol{k}) = I(-\boldsymbol{k})$. The optical orientation tilts the electron spin toward the photon spin (i.e. along $-z$) [24]; it is so strong that s_z exceeds the Rashba component s_y and the very weak s_x by far. To be more specific, s_z is as large as 80% close to the Dirac point and s_x reads 40% for s_y at $(E, k) = (-0.91\,\text{eV}, -0.156\,a_0^{-1})$; (note the decreasing color saturation in (b) via (c)–(d)). This means that optical orientation can (almost) fully align the electron's spin to the photon spin even if the initial state's spin polarization is perpendicular to the photon spin.

When changing the polar angle of incidence from 0° (setup $\mathcal{A}$) to 45° (setup $\mathcal{B}$) in the xz plane, the intensity from the DSS increases (compare the DSS in figure 2(a) with that in (e)). Due to the off-normal incidence, one would expect an intensity asymmetry in the polar angle of detection ($\vartheta_\text{e} \leftrightarrow -\vartheta_\text{e}$ or $\boldsymbol{k} \leftrightarrow -\boldsymbol{k}$). This effect is apparently minute for this surface state. The s_z component of the spin polarization becomes reduced but s_x becomes sizably large ((f), (h)). But more strikingly, the Rashba component is 'restored' (compare figure 2(g) with figure 1(c)); it shows the largest degree of spin polarization of all Cartesian components. More precisely: $\boldsymbol{s} = (-43\%, +87\%, -19\%)$ at $(E, k) = (-1.15\,\text{eV}, 0.045\,a_0^{-1})$ in (f)–(h). This implies that the degree of spin polarization is larger for the photoelectron ($|\boldsymbol{s}| = 99\%$) than for the initial state ($s_y = |\boldsymbol{s}| = +85\%$ at the same (E, k) in figure 1(c)).

Setup $\mathcal{A}$ and in particular setup $\mathcal{B}$ are suited to investigate the Rashba component of the surface state's spin texture. Although optical orientation affects the photoelectron's spin, the initial state's spin polarization can be distinguished from that due to optical orientation because there is no dichroism. In case of non-zero dichroism, the analysis can be extended as follows.

Spin-resolved experiments and calculations for dichroism provide a set of four spectra for a chosen spin quantization axis μ:

$$I(\sigma_+, \uparrow_\mu) = \frac{1}{2}\left[1 + P_\mu^\text{is} + P_\mu^\text{oo}\right] I(\sigma_+), \quad I(\sigma_+, \downarrow_\mu) = \frac{1}{2}\left[1 - P_\mu^\text{is} - P_\mu^\text{oo}\right] I(\sigma_+), \tag{5a}$$

$$I(\sigma_-, \uparrow_\mu) = \frac{1}{2}\left[1 + P_\mu^\text{is} - P_\mu^\text{oo}\right] I(\sigma_-), \quad I(\sigma_-, \downarrow_\mu) = \frac{1}{2}\left[1 - P_\mu^\text{is} + P_\mu^\text{oo}\right] I(\sigma_-) \tag{5b}$$

with the spin-integrated photocurrents $I(\sigma_\pm) \equiv I(\sigma_\pm, \uparrow_\mu) + I(\sigma_\pm, \downarrow_\mu)$. Here, we have decomposed the photoelectron's polarization into a part associated with the spin polarization

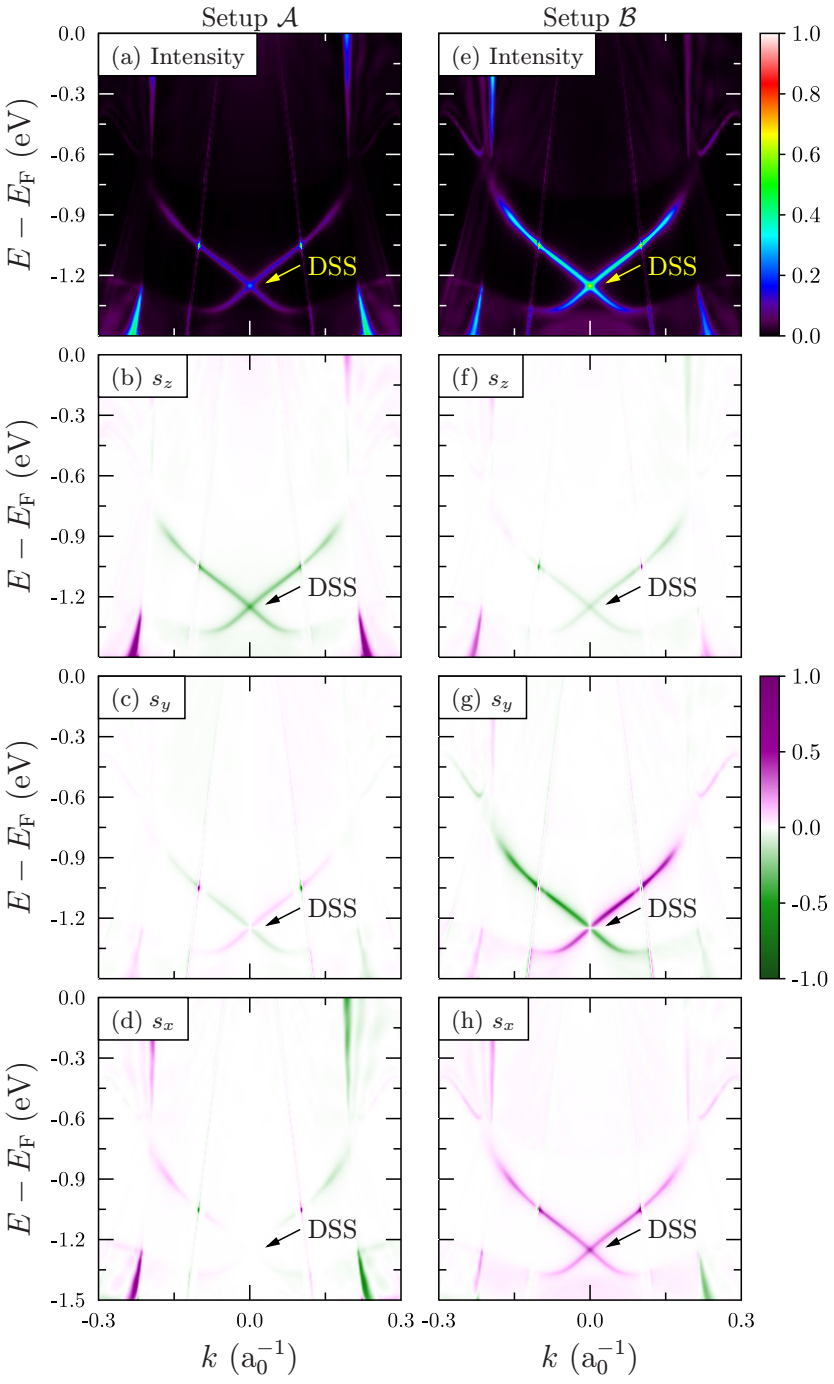

Figure 2. Spin-resolved photoemission from W(110) for wavevector $\boldsymbol{k}$ along $\overline{\mathrm{H}}$– $\overline{\Gamma}$– $\overline{\mathrm{H}}$ (k_x). Circularly polarized light with a photon energy of 21.22 eV and with helicity σ_+ impinges normally (setup $\mathcal{A}$, left column) or off-normally under $\vartheta_{\mathrm{ph}} = 45^\circ$ (setup $\mathcal{B}$, right column) onto the surface. The spin-integrated intensities (top row) are resolved with respect to s_z (second row), the 'Rashba component' s_y (third row) and s_x (bottom row). The green–white–purple color scale represents negative–zero–positive values. DSS marks the DSS.

of the initial state (is) and a part due to the optical orientation (oo), $P_\mu(\sigma_\pm) \equiv P_\mu^{\rm is} \pm P_\mu^{\rm oo}$. $P_\mu^{\rm is}$ does not change sign upon helicity reversal but $P_\mu^{\rm oo}$ does. Thus, the differences

$$D^{\rm cd} \equiv I(\sigma_+, \uparrow_\mu) + I(\sigma_+, \downarrow_\mu) - I(\sigma_-, \uparrow_\mu) - I(\sigma_-, \downarrow_\mu), \tag{6a}$$

$$D_\mu^{\rm oo} \equiv I(\sigma_+, \uparrow_\mu) - I(\sigma_+, \downarrow_\mu) - I(\sigma_-, \uparrow_\mu) + I(\sigma_-, \downarrow_\mu), \tag{6b}$$

$$D_\mu^{\rm is} \equiv I(\sigma_+, \uparrow_\mu) - I(\sigma_+, \downarrow_\mu) + I(\sigma_-, \uparrow_\mu) - I(\sigma_-, \downarrow_\mu) \tag{6c}$$

can be expressed as

$$D^{\rm cd} = I(\sigma_+) - I(\sigma_-), \tag{7a}$$

$$D_\mu^{\rm oo} = P_\mu^{\rm is}\left[I(\sigma_+) - I(\sigma_-)\right] + P_\mu^{\rm oo}\left[I(\sigma_+) + I(\sigma_-)\right], \tag{7b}$$

$$D_\mu^{\rm is} = P_\mu^{\rm is}\left[I(\sigma_+) + I(\sigma_-)\right] + P_\mu^{\rm oo}\left[I(\sigma_+) - I(\sigma_-)\right]. \tag{7c}$$

If the measure $D^{\rm cd}$ of the circular dichroism vanishes, then $D_\mu^{\rm oo}$ and $D_\mu^{\rm is}$ allow to disentangle the origin of the spin polarization component μ. To make this point more clear, consider a 'non-dichroic' setup ($\mathcal{A}$ or $\mathcal{B}$). From symmetry considerations and calculated photocurrents, we find $I(\sigma_+, \uparrow_z) = I(\sigma_-, \downarrow_z)$ and $I(\sigma_+, \downarrow_z) = I(\sigma_-, \uparrow_z)$ but $I(\sigma_+, \uparrow_y) = I(\sigma_-, \uparrow_y)$ and $I(\sigma_+, \downarrow_y) = I(\sigma_-, \downarrow_y)$. Hence, $D^{\rm cd} = D_y^{\rm oo} = D_z^{\rm is} = 0$ and $D_z^{\rm oo} \neq 0$ and $D_y^{\rm is} \neq 0$, indicating that s_z is due to optical orientation and s_y is due to the initial state.

We apply this approach to disentangle the spin polarization in the 'dichroic' setup $\mathcal{C}$ ($\overline{\rm S}$– $\overline{\Gamma}$– $\overline{\rm S}$ azimuth). The circular dichroism $D^{\rm cd}$ is non-zero (intensity asymmetry of 51% at $(E, k) = (-1.15\,{\rm eV}, 0.05\,a_0^{-1})$ in figure 3(a)) and asymmetric with respect to k. It is restricted to the DSS (DSS in figure 3(a)) because this is the electronic state with largest degree of spin polarization (figure 1(f)). The 'optical orientation' $D_\mu^{\rm oo}$ provides for both spin components—z (b) and the Rashba component R (c)—a minor background (no change of sign for the DSS), in contrast to the 'initial state' differences $D_\mu^{\rm is}$ (change of sign with k in (d) and (e)). Most strikingly, the absolute value is largest for $D_{\rm R}^{\rm is}$, as seen by the color saturation, suggesting that $s_{\rm R}$ is mainly due to the initial-state spin polarization.

Eventually, we briefly address calculated spectra for unpolarized light (not shown here). Because unpolarized light is an incoherent superposition of left- and right-handed circularly polarized light, the photocurrent shows non-zero spin polarization only in the Rashba components; the components brought about by the optical orientation vanish. For the setups $\mathcal{A}$ and $\mathcal{B}$, the spin-integrated and the s_y-resolved intensities are very similar to those shown in figure 2; s_x and s_z are zero. The similarity holds also for setup $\mathcal{C}$: spin-resolved spectra compare well with the data shown in figures 3(d) and (e).

The spin–orbit interaction couples the orbital and the spin degrees of freedom. For the mirror-symmetric setups $\mathcal{A}$ and $\mathcal{B}$, strict relations between the parity of the spatial part and the spin orientation of a wavefunction hold (confer (8) below). Thus, a measurement of the spin texture by spin-resolved photoemission allows to conclude on the parity of the initial state. It turns out that the spin texture of the Dirac surface state is connected with even orbitals, in agreement with the spectral density in which d_{z^2} orbitals show the largest contribution [15, 16]. While such an entanglement procedure is comparably simple for W(110), it becomes complicated for chalcogenide topological insulators. Nevertheless, Zhu *et al* [44] have successfully analyzed spin texture and orbital composition of the Dirac surface state in Bi_2Se_3, using an analysis similar to that presented here.

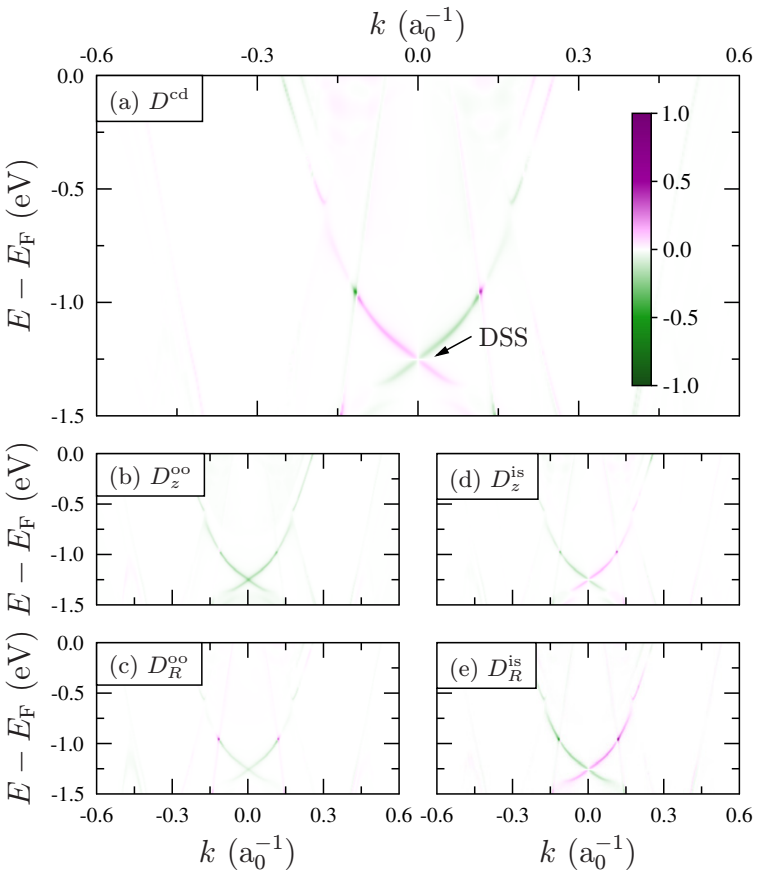

Figure 3. Dichroic photoemission from W(110) for wavevector $\boldsymbol{k}$ along $\overline{\text{S}}$– $\overline{\Gamma}$– $\overline{\text{S}}$ (setup $\mathcal{C}$, see text). Top: dichroism D^{cd}. DSS marks the DSS. Bottom: D_μ^{oo} and D_μ^{is} for the out-of-plane ($\mu = z$, (b) and (d)) and the Rashba ($\mu = R$, (c) and (e)) spin components. Parameters as for figure 2.

3.3. (e, 2e)

Complementary to photoemission, electron-induced two-electron emission is also a powerful tool for studying the spin–orbit-induced spin texture at surfaces. We demonstrate this for the case of the surface electronic structure of W(110) in the $\overline{\text{H}}$– $\overline{\Gamma}$– $\overline{\text{H}}$ azimuth, for which the scattering plane—xz—is a mirror plane of the semi-infinite crystal. Due to spin–orbit coupling, all four one-electron states have the schematic forms [40]

$$|\text{even}, \uparrow_y\rangle + |\text{odd}, \downarrow_y\rangle, \quad |\text{even}, \downarrow_y\rangle + |\text{odd}, \uparrow_y\rangle, \tag{8}$$

where 'even' and 'odd' indicate spatial parts of even and odd parity with respect to the xz plane of the semi-infinite crystal; the spinor parts are quantized with respect to the Rashba component $\mu = y$.[8] Since the primary and the two outgoing electron states are predominantly even, a selection rule [45] holds in good approximation: only the even parts of the valence states enter the $(e, 2e)$ matrix elements.

[8] To be consistent with the usual nomenclature in $(e, 2e)$, we replace $\uparrow$ by + (spin up) and $\downarrow$ by − (spin down) in the following.

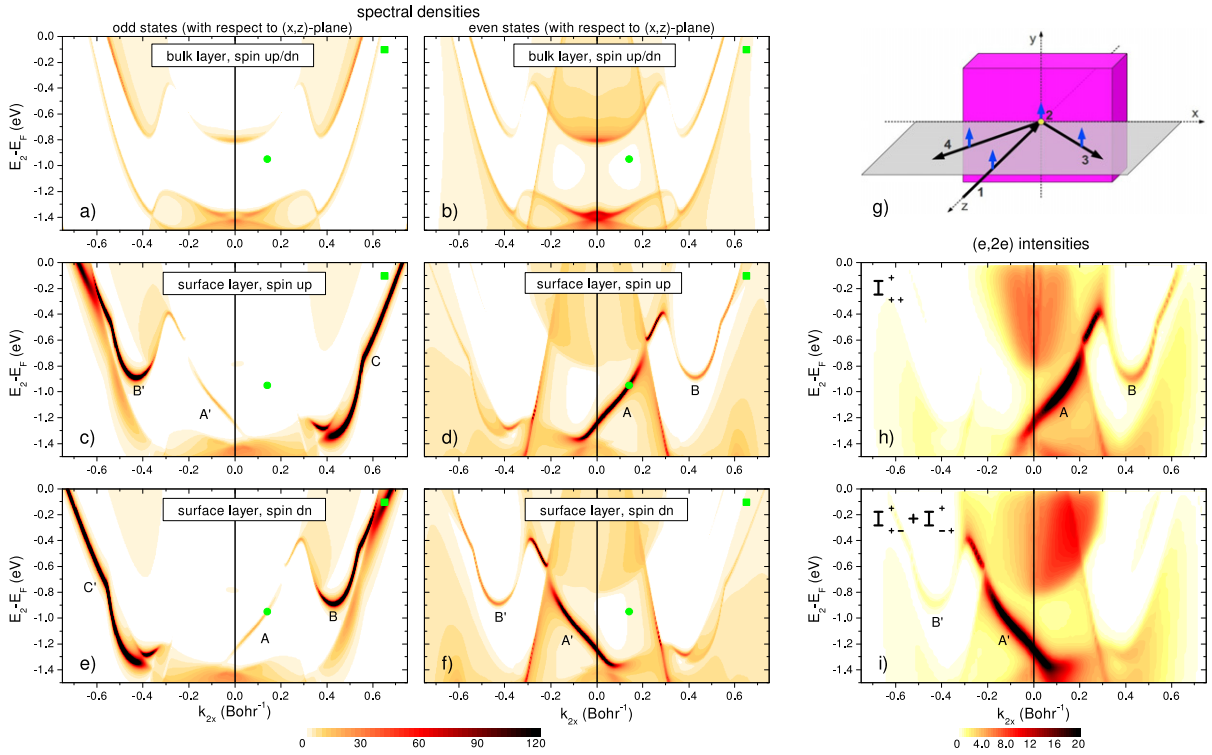

Figure 4. $(e, 2e)$ from W(110) in the $\overline{\text{H}}$– $\overline{\Gamma}$– $\overline{\text{H}}$ azimuth. Left: spectral densities of a bulk layer ((a), (b)) and of the topmost surface layer resolved with respect to the Rashba spin component $s_{\text{R}} = s_y$ and spatial parity (odd: (a), (c), (e); even: (b), (d), (f)), as indicated in each panel (c)–(f). Green symbols mark (E, k) positions of valence states studied in figure 5. Right: sketch of the $(e, 2e)$ setup (g) and associated spin-resolved $(e, 2e)$ intensities $I^{+}_{\sigma_3\sigma_4}$ ((h), (i)); $E_1 = 25\,\text{eV}$, $\boldsymbol{k}_1 = 0$, $\vartheta_{3,4} = 50^\circ$.

The left-hand part of figure 4 shows spectral densities for a bulk layer ((a), (b)) and the topmost surface layer (c)–(f) resolved with respect to spatial symmetry and spin. From panels (c)–(f) it is apparent that the branches of the DSS (labeled A and A′ for positive and negative k_{2x}, respectively) are almost exclusively even and spin-polarized. The surface state branches B, B′, C and C′ are also strongly spin-polarized but of predominantly odd parity.

For normally incident primary electrons and emission at equal polar angles (figure 4(g)), the conservation conditions 4 turn the $(e, 2e)$ intensities $I^{\sigma_1}_{\sigma_3,\sigma_4}$ into functions of the valence electron energy E_2 and its parallel momentum component k_{2x}. These are shown for primary spin $\sigma_1 = +$ in figures 4(h) and (i). The parallel-spin intensity I^{+}_{++} in panel (h) maps the spin-up even-parity surface state spectral density shown in panel (d), whereas the antiparallel-spin intensity $I^{+}_{+-} + I^{+}_{-+}$ in panel (i) reflects the spin-down even-parity spectral density of panel (f). Since the mirror operation at the yz plane reverses all the spins, the intensities I^{-}_{--} and $I^{-}_{-+} + I^{-}_{+-}$ are the mirror images of I^{+}_{++} and $I^{+}_{+-} + I^{+}_{-+}$, respectively.

The strong spin polarization of the DSS facilitates an investigation of the spin dependence of the exchange-correlation hole. For this purpose, an $(e, 2e)$ setup is suitable, in which the two emitted electrons have fixed equal energies $E_3 = E_4$ and variable surface-parallel momenta,

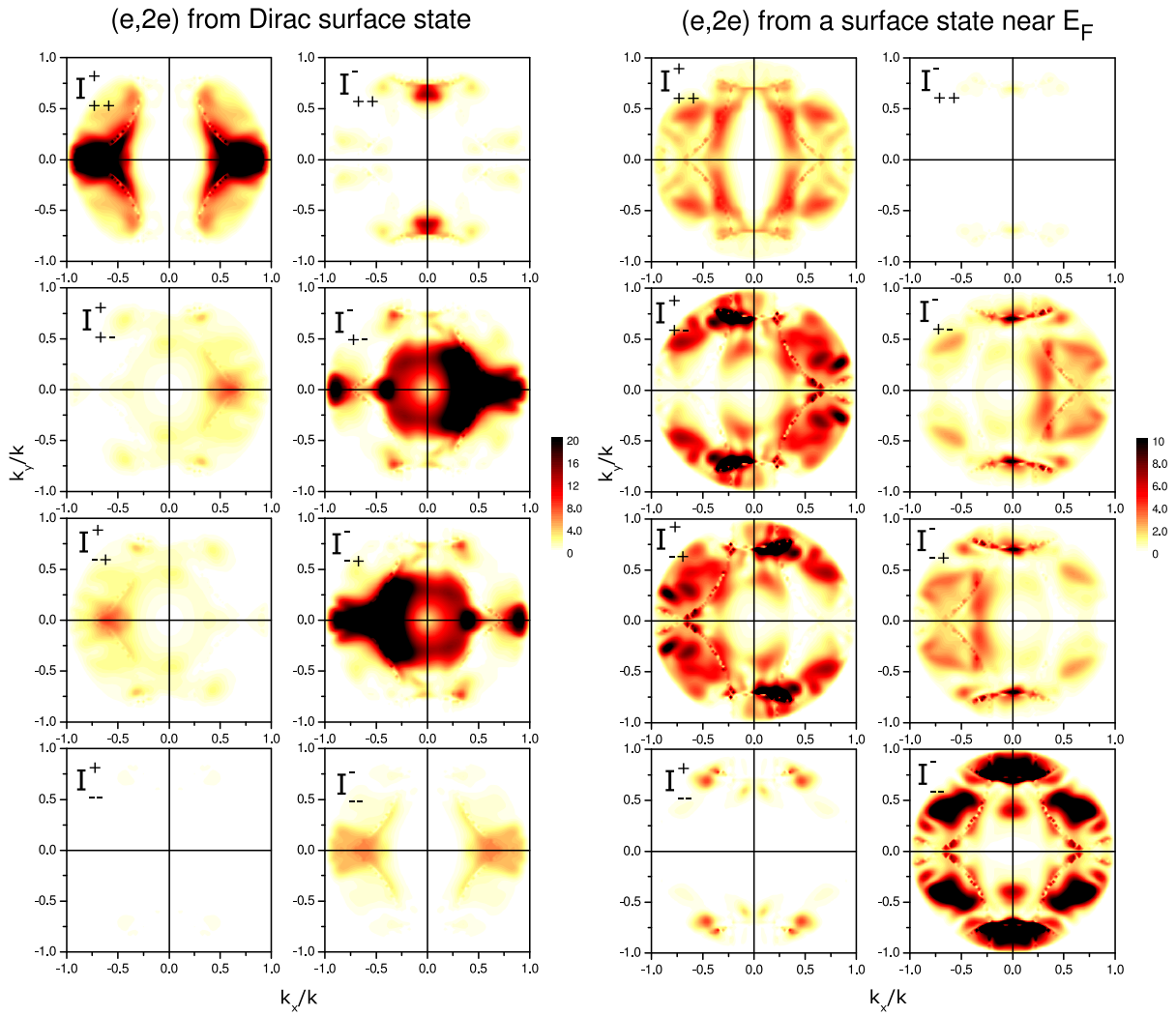

Figure 5. $(e, 2e)$ momentum distributions $I^{\sigma_1}_{\sigma_3\sigma_4}(k_x, k_y)$ from W(110), with spins $\sigma_i = \pm$ along the y-axis as indicated in each panel. Left: valence electrons from the Dirac surface state with (E_2, k_{2x}) marked by green dots in figure 4. Right: valence electron from another surface state with (E_2, k_{2x}) marked by green squares in figure 4. For details see text.

$\boldsymbol{k}_3 = -\boldsymbol{k}_4$. By virtue of energy and momentum conservation (4) a surface state electron with E_2 and $\boldsymbol{k}_2$ can then be selected by choosing for the primary electron $E_1 = E_3 + E_4 - E_2$ and $\boldsymbol{k}_1 = -\boldsymbol{k}_2$. As a typical example, we select the point $(E_2 = E_\mathrm{F} - 0.95\,\mathrm{eV}, \boldsymbol{k}_2 = (+0.142, 0)\, a_0^{-1})$ on the spin-up branch of the DSS, which is indicated by the green dot in the left-hand part of figure 4. The primary electron with an energy $E_1 = 25\,\mathrm{eV}$ is incident with parallel momentum $\boldsymbol{k}_1 = (-0.142, 0)\, a_0^{-1}$ (i.e. within the $\overline{\mathrm{H}}$– $\overline{\Gamma}$– $\overline{\mathrm{H}}$ azimuth at $\vartheta_1 = 6.01^\circ$ and $\varphi_1 = 180^\circ$). The emitted electrons have energies of $E_3 = E_4 = 9.49\,\mathrm{eV}$ and surface-parallel momenta $\boldsymbol{k}_3 = -\boldsymbol{k}_4$.

The resulting $(e, 2e)$ momentum distributions $I^{\sigma_1}_{\sigma_3\sigma_4}(k_x, k_y)$ in the plane $\boldsymbol{k}/k \equiv \boldsymbol{k}_3/\sqrt{2E_3} = -\boldsymbol{k}_4/\sqrt{2E_4}$ (with $E_3 = E_4$ in Hartree atomic units) of the outgoing electrons are shown in the left-hand part of figure 5. For primary spin up ($\sigma_1 = +$), the parallel-spin intensity I^+_{++}

exhibits a large central depletion zone which is due to exchange and Coulomb correlation. The antiparallel-spin intensities are by far smaller. For primary spin down ($\sigma_1 = -$), the antiparallel-spin intensities dominate and show a rather small central 'hole' which is due to Coulomb correlation only. The apparently spin-non-conserving intensities I^{+}_{--} and I^{-}_{++} rely on spin–orbit coupling in the primary and outgoing electron states; in fact they vanish in calculations without spin–orbit coupling in these states. The sums of the intensities $I^{\sigma_1}_{\sigma_3\sigma_4}$ over the outgoing-electron spin orientations σ_3 and σ_4 still exhibit, for primary spin $\sigma_1 = +$, the large exchange-correlation hole and, for $\sigma_1 = -$, the smaller correlation hole. Exchange and correlation effects can thus be disentangled in experiments *without* resolving the spins of the emitted electrons.

In the right-hand part of figure 5, we show analogous momentum distributions obtained for the valence electron surface state with $E_2 = E_F - 0.10\,\text{eV}$ and $\boldsymbol{k}_2 = (0.65, 0)\,a_0^{-1}$ (green square in the left-hand part of figure 4), which is selected using primary electrons with $E_1 = 25\,\text{eV}$ incident at $\vartheta_1 = 28.61^\circ$ and $\varphi_1 = 180^\circ$. Again, the parallel-spin distributions exhibit an exchange-correlation hole which is larger than the correlation hole in the antiparallel-spin distributions.

A striking difference between the $(e, 2e)$ intensities from the DSS and those from the other spin-polarized surface state is that the former are strongest around the k_x-axis, whereas the latter are very small along this axis. This is explained by the different spatial symmetry of the two states (see figure 4). For the outgoing electrons in the xz plane, the above-mentioned selection rule favors states with predominant even parity (like the DSS). For emission in planes other than xz, odd-parity parts of valence states also contribute to the intensities.

4. Concluding remarks

As we have shown by calculations of photo- and electron-pair emission, W(110) could serve as an important system for investigating experimentally spin–orbit effects in electron spectroscopies. Hence, it is obvious to study other non-magnetic metals with bcc structure. The strength of the spin–orbit interaction could be studied by comparing W(110) ($Z = 74$) with Mo(110) ($Z = 42$). Another topic is whether *unoccupied* strongly spin-polarized surface states exist at bcc(110) surfaces [46]; these could be investigated by spin-resolved inverse photoemission, two-photon photoemission or scanning tunneling spectroscopy [47–50].

Acknowledgments

We thank M Donath (University Münster) for very fruitful discussions. This work was supported by the Priority Program 1666 of the DFG.

References

[1] Hasan H and Kane C 2010 Colloquium: topological insulators *Rev. Mod. Phys.* **82** 3045
[2] Fu L, Kane C L and Mele E J 2007 Topological insulators in three dimensions *Phys. Rev. Lett.* **98** 106803
[3] Bychkov Y A and Rashba E I 1984 Oscillatory effects and the magnetic susceptibility of carriers in inversion layers *J. Phys. C: Sol. State Phys.* **17** 6039
[4] Bychkov Yu A and Rashba É I 1984 Properties of a 2D electron gas with lifted degeneracy *Sov. Phys.—JETP Lett.* **39** 78

[5] Winkler R 2003 *Spin-Orbit Coupling Effects in Two-Dimensional Electron and Hole Systems* (Berlin: Springer)
[6] Fu L 2011 Topological crystalline insulators *Phys. Rev. Lett.* **106** 106802
[7] Hsieh T H, Lin H, Liu J, Duan W, Bansil A and Fu L 2012 Topological crystalline insulator in the SnTe material class *Nature Commun.* **3** 982
[8] Chadov St, Kiss J, Felser C, Chadova K, Ködderitzsch D, Minár J and Ebert H 2012 Topological phase transition induced by random substitution arXiv:1207.3463v1
[9] Di Sante D, Barone P, Bertacco R and Picozzi S 2012 Electric control of giant Rashba effect in bulk GeTe *Adv. Mater.* **25** 509–13
[10] Miyamoto K, Kimura A, Kuroda K, Okuda T, Shimada K, Namatame H, Taniguchi M and Donath M 2012 Spin-polarized Dirac-cone-like surface state with *d* character at W(110) *Phys. Rev. Lett.* **108** 066808
[11] Miyamoto K, Kimura A, Okuda T, Shimada K, Iwasawa H, Hayashi H, Namatame H, Taniguchi M and Donath M 2012 Massless or heavy due to two-fold symmetry: surface-state electrons at W(110) *Phys. Rev.* B **86** 161411
[12] Rybkin A G, Krasovskii E E, Marchenko D, Chulkov E V, Varykhalov A, Rader O and Shikin A M 2012 Topology of spin polarization of the 5d states on W(110) and Al/W(110) surfaces *Phys. Rev.* B **86** 035117
[13] Rotenberg E, Chung J W and Kevan S D 1999 Spin–orbit coupling induced surface band splitting in Li/W(110) and Li/Mo(110) *Phys. Rev. Lett.* **82** 4066
[14] Kevan S V (ed) 1992 *Angle-Resolved Photoemission: Theory and Current Applications* (Amsterdam: Elsevier) chapters 1 and 2
[15] Giebels F, Gollisch H and Feder R 2013 Electron pair emission from W(110): response to a spin-polarized surface state *Phys. Rev.* B **87** 034124
[16] Mirhosseini H, Flieger M and Henk J 2013 Dirac-cone-like surface state in W(110): dispersion, spin texture, and photoemission from first principles *New J. Phys.* **15** 033019
[17] Kirschner J 1985 *Polarized Electrons at Surfaces* (London: Springer)
[18] Kessler J 1985 *Polarized Electrons* 2nd edn (*Springer Series on Atoms and Plasmas* vol 1) ed G Ecker, P Lambropoulos and H Walther (Berlin: Springer) chapter 3
[19] Feder R (ed) 1985 *Polarized Electrons in Surface Physics (Advanced Series in Surface Science)* (Singapore: World Scientific) chapters 4, 6, 7, 9, 10, 11, 12 and 13
[20] Schattke W 1997 Photoemission within and beyond the one-step model *Prog. Surf. Sci.* **54** 211
[21] Schattke W and van Hove M A (ed) 2003 *Solid-State Photoemission and Related Methods. Theory and Experiment* (Weinheim: Wiley-VCH) chapter 5
[22] Feder R and Gollisch H 2003 Low energy $(e, 2e)$ spectroscopy *Solid State Photoemission and Related Methods* ed W Schattke and M A van Hove (Weinheim: Wiley-VCH) chapter 9, p 269
[23] Berakdar J and Kirschner J (ed) 2004 *Correlation Spectroscopy of Surfaces, Thin Films, and Nanostructures* (Weinheim: Wiley-VCH) chapters 5, 6 and 9
[24] Fano U 1968 Spin orientation of photoelectrons ejected by circularly polarized light *Phys. Rev.* **178** 131
[25] Hsieh D *et al* 2009 Observation of unconventional quantum spin textures in topological insulators *Science* **323** 919
[26] Hasan M Z and Moore J E 2011 Three-dimensional topological insulators *Annu. Rev. Condens. Matter Phys.* **2** 55
[27] Henk J, Ernst A, Eremeev S V, Chulkov E C, Maznichenko I V and Mertig I 2012 Complex spin texture in the pure and Mn-doped topological insulator Bi_2Te_3 *Phys. Rev. Lett.* **109** 036803
[28] Scholz M R, Marchenko D, Varykhalov A, Volykhov A, Yashina L V and Rader O 2011 High spin polarization and circular dichroism of topological surfaces states on Bi_2Te_3 arXiv:1108.1053v1
[29] Wang Y H, Hsieh D, Pilon D, Fu L, Gardner D R, Lee Y S and Gedik N 2011 Observation of a warped helical spin texture in Bi_2Se_3 from circular dichroism angle-resolved photoemisison spectroscopy *Phys. Rev. Lett.* **107** 207602
[30] Heinzmann U and Dil J H 2012 Spin–orbit-induced photoelectron spin polarization in angle-resolved photoemission from both atomic and condensed matter *J. Phys.: Condens. Matter* **24** 173001

[31] Henk J 2002 Theory of low-energy diffraction and photoelectron spectroscopy from ultra-thin films *Handbook of Thin Film Materials* vol 2 ed H S Nalwa (San Diego, CA: Academic) chapter 10, p 479
[32] Zabloudil J, Hammerling R, Szunyogh L and Weinberger P (ed) 2005 *Electron Scattering in Solid Matter* (Berlin: Springer) chapters 1 and 10
[33] Venus D, Cool S and Plihal M 2000 Quantitative structural determination using spin-polarized low-energy electron diffraction rotation curves: W(110) *Surf. Sci.* **446** 199
[34] Meyerheim H L, Sander D, Popescu R, Steadman P, Ferrer S and Kirschner J 2001 Interlayer relaxation of W(110) studied surface x-ray diffraction *Surf. Sci.* **475** 103
[35] Rundgren J and Malmström G 1977 Transmission and reflection of low-energy electrons at the surface barrier of a metal *J. Phys. C: Sol. State Phys.* **10** 4671–87
[36] Braun J 1996 The theory of angle-resolved ultra-violet photoemission and its applications to ordered materials *Rep. Prog. Phys.* **59** 1267
[37] Braun J and Donath M 2004 Theory of photoemission from surfaces *J. Phys.: Condens. Matter* **16** S2539
[38] Henk J and Johansson B 1998 Magnetic dichroism in off-normal valence-band photoemission *J. Electron. Spectrosc. Relat. Phenom.* **94** 259
[39] Gollisch H, von Schwartzenberg N and Feder R 2006 Emission of correlated electron pairs from solid surfaces *Phys. Rev.* B **74** 075407
[40] Inui T, Tanabe Y and Onodera Y 1990 *Group Theory and its Applications in Physics* (*Springer Series in Solid State Sciences* vol 78) ed M Cardona, P Fulde, K von Klitzing and H-J Queisser (Berlin: Springer) chapter 12
[41] Eremeev S V *et al* 2012 Atom-specific spin mapping and buried topological states in a homological series of topological insulators *Nature Commun.* **3** 635
[42] Fu L 2009 Hexagonal warping effects in the surface state of the topological insulator Bi_2Te_3 *Phys. Rev. Lett.* **103** 266801
[43] Susmita Basak, Hsin Lin, Wray L A, Xu S-Y, Fu L, Hasan M Z and Bansil A 2011 Spin texture of the warped Dirac-cone surface states in topological insulators *Phys. Rev.* B **84** 121401
[44] Zhu Z-H, Veenstra C N, Levy G, Ubaldini A, Syers P, Butch N P, Paglione J, Haverkort M W, Elfimov I S and Damascelli A 2013 Layer-by-layer entangled spin–orbital texture of the topological surface state in Bi_2Se_3 *Phys. Rev. Lett.* **110** 216401
[45] Feder R and Gollisch H 2001 Selection rules in $(e, 2e)$ spectroscopy from surfaces *Solid State Commun.* **119** 625
[46] Niesner D *et al* 2012 Unoccupied topological states on bismuth chalcogenides *Phys. Rev.* B **86** 205403
[47] Donath M 1990 Polarization effects in inverse photoemission spectra *Prog. Surf. Sci.* **35** 47
[48] Schattke W, Krasovskii E E, Díez Muiño R and Echenique P M 2008 Direct resolution of unoccupied states in solids via two-photon photoemission *Phys. Rev.* B **78** 155314
[49] Chiang C-T, Winkelmann A, Yu P, Kirschner J and Henk J 2010 Spin–orbit coupling in unoccupied quantum well states: experiment and theory for Co/Cu(001) *Phys. Rev.* B **81** 115130
[50] Akin Ünal A, Tusche C, Quazi S, Wedekind S, Chiang C-T, Winkelmann A, Sander D, Henk J and Kirschner J 2011 Hybridization between the unoccupied Shockley surface state and bulk electronic states on Cu(111) *Phys. Rev.* B **84** 073107